JOURNAL OF Materials CHEMISTRY

The widespread occurrence of negative thermal expansion in zeolites†

Philip Lightfoot,* David A. Woodcock, Martin J. Maple, Luis A. Villaescusa and Paul A. Wright

School of Chemistry, University of St Andrews, St Andrews, Fife, UK KY16 9ST. E-mail: pl@st-and.ac.uk; Fax: +44 (0)1334 463808

Received 25th April 2000, Accepted 29th June 2000
First published as an Advance Article on the web 6th October 2000

Powder X-ray and neutron diffraction studies of the calcined siliceous zeolites ITQ-7, ITQ-9 and CIT-5, and the aluminophosphates $AlPO_4$-31 and Mg-doped $AlPO_4$-17 have been carried out as a function of temperature in order to determine their thermal expansivity properties. Of these, ITQ-7, ITQ-9 and MAPO-17 show negative thermal expansivity over a wide temperature range, in common with several other previously studied microporous materials. CIT-5 and $AlPO_4$-31 are anomalous in showing an expansion on heating. A detailed study of CIT-5 highlights the key structural parameters which determine its positive expansivity. From expansivity data currently available on seventeen microporous materials, it is clear that negative thermal expansivity must be considered the norm rather than the exception. Positive expansivity is encouraged by the structure having a relatively high framework density and a one-dimensional channel system.

Introduction

There has recently been renewed interest in materials exhibiting the unusual phenomenon of negative thermal expansion (NTE), *i.e.* materials which *contract* on heating. This phenomenon arises, in general terms, from a secondary structural or dynamic mechanism which overrides the normal thermal expansivity of chemical bonds. In detail, the mechanism of this behaviour is not yet understood for all the systems in which it occurs, but several contributing effects have been highlighted, for example, ferroelectric (*e.g.* $PbTiO_3$) and magnetostrictive (*e.g.* Invar) phase transitions and low-frequency phonon modes, specifically transverse vibrations of two-coordinated atoms and cooperative motions of linked quasi-rigid polyhedral units (so-called 'rigid-unit modes' or RUMs, for example, in β-quartz). An excellent introduction to some of these phenomena, and examples of some of the materials exhibiting them, has recently been given by Evans.[1] Among the materials exhibiting NTE, framework oxides represent a large sub-class; mixed oxides such as ZrW_2O_8,[2,3] ZrP_2O_7[4] and the Nasicon or NZP family[5,6] have recently been studied in this respect. A further class of oxidic materials are the microporous framework materials encompassing silicate zeolites and aluminophosphates. Our interest in these materials arose from the theoretical predictions of NTE in zeolites by Tschaufeser and Parker.[7] Experimental verification of NTE in some of these materials has been provided by Couves *et al.*[8] for zeolite X, Park *et al.* for several pure silica zeolites,[9] Attfield and Sleight for siliceous faujasite[10] and $AlPO_4$-17,[11] and our own work on the pure silica polymorphs ITQ-1, ITQ-3 and SSZ-23[12] and also siliceous chabazite and ITQ-4.[13] In this paper we report further examples of NTE, determined by powder X-ray and neutron diffraction methods, in the new SiO_2 polymorphs ITQ-7 and ITQ-9 and in a magnesium-doped $AlPO_4$-17 (MAPO-17) phase, and contrast these with the observation of positive thermal expansivity in the large-pore SiO_2 polymorph CIT-5 and $AlPO_4$-31. In all of these systems, except zeolite X and MAPO-17, there are no extra-framework cations or other species, and the frameworks themselves are electrostatically neutral. The cumulative data so far point towards the conclusion that NTE in microporous oxides is the norm rather than the exception.

†Basis of a presentation given at Materials Discussion No. 3, 26–29 September, 2000, University of Cambridge, UK.

Experimental

Pure polycrystalline samples of the SiO_2 polymorphs ITQ-7,[14] ITQ-9[15] and CIT-5[16] were provided by Dr M. A. Camblor and co-workers (Valencia). $AlPO_4$-31 was prepared by literature methods.[17] A magnesium-substituted $AlPO_4$-17 derivative of framework composition $Mg_{0.1}Al_{0.9}PO_4$ was prepared from a gel of composition $0.4R(OH)_2 : 0.1Mg(OAc)_2 : 0.9Al(OH)_3 : H_3PO_4 : 40H_2O$, heated at 190 °C for 48 h {R represents the diquinuclidinium cation $[(C_7H_{13}N)–(CH_2)_3–(NC_7H_{13})]^{2+}$}.[18] All samples were calcined in flowing O_2 at 500 °C for several hours and subsequently stored under anhydrous conditions.

Preliminary X-ray powder diffraction data were recorded in sealed 0.5 mm glass capillaries on a Stoe STADI/P transmission-geometry diffractometer using monochromated Cu-Kα_1 radiation. For $AlPO_4$-31, additional high-temperature X-ray data were collected at 50 °C intervals for $50\,°C < T < 550\,°C$ over the 2θ range 7–45°. The variation of lattice parameters *versus* temperature was determined by Rietveld refinement (GSAS program[19]) using a fixed structural model (rhombohedral, $R\bar{3}$[20]) and refining scale factor, lattice parameters, detector zero-point, background and peak shape only. In the cases of the remaining four samples, powder neutron diffraction data were used for the thermal expansivity studies. Data for ITQ-7, CIT-5 and MAPO-17 were collected on the OSIRIS instrument[21] at the ISIS facility of the CCLRC Rutherford Appleton Laboratory. Polycrystalline samples weighing approximately 2 g were placed in vanadium cans. Measurements were recorded at 30 °C and in 100 °C steps from 100 to 700 °C for CIT-5, at 50 °C and from 100 to 500 °C in 100 °C steps for MAPO-17 and at 60 and 120 °C, and from 200 to 600 °C in 100 °C steps for ITQ-7. Problems with the incident neutron flux at 300 °C for ITQ-7 led to this measurement being discarded. A measurement of an empty can was recorded and subtracted from the initial data before starting the refinements.

 DOI: 10.1039/b002950p

This journal is © The Royal Society of Chemistry 2001

Refinements were carried out using the GSAS program. For both CIT-5 and ITQ-7, unit cell parameters, scale factor, background, peak shape (Gaussian double exponential), atomic co-ordinates and isotropic temperature factors, which were constrained by atom type, were refined. For the CIT-5 data, 57 variables and 4757 reflections over the range 1.0 to 7.0 Å were refined, and for the ITQ-7 data, 59 variables and 1860 reflections over the same *d*-spacing range. Soft constraints for Si–O (1.61 ± 0.005) and O–O (2.58 ± 0.005) distances were used.

Due to poorer data quality, MAPO-17 refinements were of scale factor, background and unit cell parameters only, using 7 variables and 4373 reflections over the range 1.0 to 7.0 Å. For ITQ-9, data were collected in a vanadium can on the POLARIS instrument at 20 °C, and from 200 to 600 °C in 100 °C steps. A background measurement was subtracted. The same refinement strategy was used as in the CIT-5 and ITQ-7 experiments, although data from the low-angle, 90° and backscattering banks were combined for greater precision. This resulted in an overall *d*-spacing range of 0.7 to 8.3 Å and refinements using 104 variables and 6135 reflections.

Results and discussion

Some basic structural features of the zeolites under study are given in Table 1. It can be seen that the complexity of these structures [in terms of the number of crystallographic variables, or number of unique tetrahedral (T) atom sites] is relatively large. For this reason, it was, unfortunately, not possible to carry out full unrestrained refinements of all the crystallographic variables and derive reliable geometric and thermal parameters. The most precise refinements were obtained in the case of CIT-5, using the restrained model described above. In this case, systematic trends can be seen in the derived structural parameters, which will be further described later. However, the most important fundamental information to be gained from these studies is the thermal expansivity data itself, in terms of axial changes in the crystallographic cell parameters. These parameters are derived very precisely and reliably from powder diffraction experiments. Typical plots of unit cell parameters *versus* temperature for CIT-5 and MAPO-17 are shown in Fig. 1 and 2. In most cases, the axial coefficients of thermal expansivity (α) were non-linear functions of temperature, but a reasonable feeling for their behaviour can be obtained by approximating to a simpler linear fit. Values of α for the relevant unit cell parameters, together with those obtained for other microporous materials from earlier powder diffraction experiments, are given in Table 2. As can be seen from these figures, the vast majority of the materials studied exhibit overall NTE throughout the temperature range studied, with most showing NTE along all three crystallographic axes. Dramatically different behaviour is, however, observed in the cases of CIT-5 and $AlPO_4$-31, which both show large positive axial α values. From Table 1, it can be seen that both of these materials adopt one-dimensional channel systems and also have relatively high framework densities; it is tempting to suggest that these may be significant factors in determining their behaviour. Indeed, Tschaufeser and Parker[7] originally predicted this possibility on the basis of computational studies of

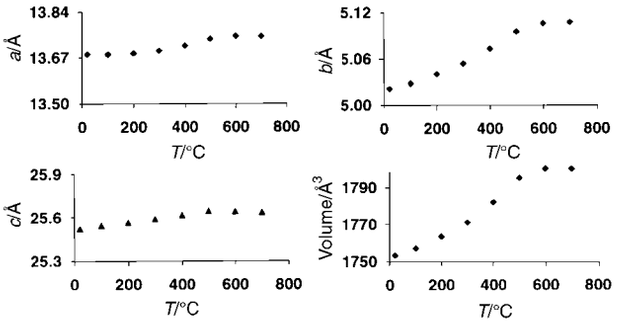

Fig. 1 Thermal evolution of lattice parameters for CIT-5.

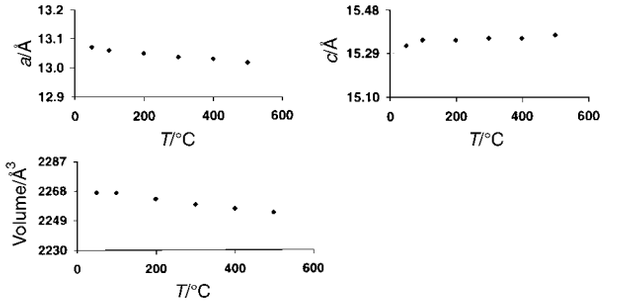

Fig. 2 Thermal evolution of lattice parameters for MAPO-17 (Note: for easy comparison of the expansivites, all the graphs in Fig. 1 and 2 are plotted on the same percentage $\Delta y/y$-scale).

the one-dimensional $AlPO_4$ systems $AlPO_4$-5, $AlPO_4$-8 and VPI-5. They suggested that the relatively high framework density *along* the channel direction would make NTE unfavourable. This also appears to be borne out by our previous observation of a positive thermal expansivity along the channel axis (average $\alpha_c \approx +7 \times 10^{-6}$ over the range $95\ \mathrm{K} < T < 510\ \mathrm{K}$) in the one-dimensional 12-MR system ITQ-4 (framework density ≈ 17.0), which overall displays NTE.[13] However, the pitfalls in comparing simulations with experimental results must be borne in mind; for example, although $AlPO_4$-5 (AFI) was predicted to show positive thermal expansivity,[7] the experimental data of Park *et al.*[9] demonstrate positive thermal expansivity only as high as 424 K, whence strong NTE ensues (Table 2). The temperature range over which the expansivity behaviour is studied, both experimentally and theoretically, is a key factor—our recent results on ITQ-4, for example, which extend the previously available data[13] to higher temperatures, show a turnaround in the α_c coefficient from positive to negative. It is also interesting to note that, for both $AlPO_4$-31 and CIT-5 (Fig. 1), the expansivity tends towards zero at the highest temperatures studied—this corresponds to a reduction of the framework density of CIT-5 from 18.3 to 17.8, and of $AlPO_4$-31 from 19.2 to 18.9 T atoms per 1000 Å^3.

It is interesting to compare our results on MAPO-17 with those for $AlPO_4$-17 (both adopting the ERI structure type) obtained by Attfield and Sleight.[11] Tschaufeser and Parker[7] originally predicted that the NTE in $AlPO_4$-17 itself should be stronger at higher temperatures, at least up to their limit of 500 K, with values ranging

Table 1 Salient structural data for the materials studied

Material	Type[a]	Space group	Channel system[b]	Approx. unit cell (*a*, *b*, *c*)/Å	Unique T sites	Framework density[c]
$AlPO_4$-31	ATO	$R\bar{3}$	1D-12MR [001]	20.8, 20.8, 5.0 (hexagonal)	2	19.2
MAPO-17	ERI	$P6_3/m$	1D-12MR [001]	13.1, 13.1, 15.3	4	15.9
ITQ-7	ISV	$P4_2/mmc$	3D-12MR	12.8, 12.8, 25.2	5	15.4
ITQ-9	STF	$I\bar{1}$	1D-10MR [001]	14.7, 18.2, 7.4	8	17.2
CIT-5	CFI	$Im2a$	1D-14MR [010]	13.7, 5.0, 25.5	5	18.3

[a]IZC structure code.[26] [b]*n*MR: *n*-membered ring (*i.e.* *n* T-sites per ring). [c]No. of T sites per 1000 Å^3.

Table 2 Known coefficients of thermal expansion for a variety of microporous solids[a]

Sample	α_a[b]	α_b	α_c	α_V	Range (T/K)	F.D.[c]	Reference
ITQ-1	−4.23	−4.23	−3.21	−12.1	323–773	16.6	12
ITQ-3	−0.29	−2.06	−10.1	−11.4	323–823	16.2	12
ITQ-4	−11.5	−7.47	+7.19	−9.1	95–510	17.0	13
ITQ-7	−2.28	−2.28	−1.05	−5.6	473–873	15.4	This work
ITQ-9	−5.58	−2.37	−2.19	−10.0	293–873	17.2	This work
SSZ-23	−6.09	−3.21	−0.73	−10.3	323–773	16.7	12
MFI	−5.5	−6.9	−2.8	−15.1	393–975	17.9	9
AFI	−5.1	−5.1	−3.7	−14.5	424–774	17.6	9
DOH	−0.6	−0.6	−3.1	−3.1	573–996	18.4	9
MTN	−1.7	−1.7	−1.7	−5.0	463–1002	18.7	9
DDR	−2.8	−2.8	−3.1	−8.7	492–1185	17.8	9
FAU	−4.2	−4.2	−4.2	−12.6	25–573	13.5	10
MAPO-17	−9.16	−9.16	+4.66	−4.6	323–773	15.9	This work
$AlPO_4$-17	−15.3	−15.3	−4.52	−35.1	18–300	15.8	11
CHA	−8.24	−8.24	−13.3	−28.5	293–873	15.4	13
CIT-5	+8.57	+28.2	+8.41	+14.9	373–973	18.3	This work
$AlPO_4$-31	+9.72	+9.72	+17.3	+32.8	323–823	19.2	This work

[a]The quoted values are taken as the average linear expansivities—in some cases the true behaviour is significantly non-linear. [b]α_l is defined as $\Delta l/l\Delta T$ in units of $10^{-6}\,^{\circ}C^{-1}$. [c]F.D.: framework density (no. of T sites per 1000 Å^3) at room temp.

from about $\alpha(\text{average}) \approx -12 \times 10^{-6}\,^{\circ}C^{-1}$ at 50 K to $-30 \times 10^{-6}\,^{\circ}C^{-1}$ at 500 K. Attfield and Sleight reported a nearly constant $\alpha(\text{average})$ ($=1/3\alpha_v$) of $-11.7 \times 10^{-6}\,^{\circ}C^{-1}$ over the range 18–300 K, although α_c does appear to become less negative at the higher limit. Our own data on MAPO-17 (Table 2) over the temperature range 323–773 K are in marked contrast to either of these reports, with approximately linear behaviour of both axes, and an $\alpha(\text{average})$ of only $-1.5 \times 10^{-6}\,^{\circ}C^{-1}$; the most significant difference is that the *c*-axis actually *expands* throughout this temperature range. This difference, at least in part, must be ascribed to the presence of 10% divalent Mg^{2+} substituting for Al^{3+} throughout the framework in MAPO-17. After calcination, the charge deficiency that results is largely made up of charge-balancing protons on bridging oxygens (so-called 'bridging hydroxyls'). Clearly, subtle differences in framework composition can have a considerable influence on expansivity behaviour, and this must be considered in future work.

Thermal expansion in CIT-5

As we have shown above, siliceous CIT-5 represents a rare example of a microporous solid which actually *expands* on heating, having a particularly large expansivity along the one-dimensional channel axis, *b*. Our restrained refinements from powder neutron diffraction data produce well-behaved structural parameters and, we believe, permit us to identify some of the key parameters underlying the structural origin of this perhaps anomalous behaviour. The calcined form of CIT-5 was first reported to adopt the centrosymmetric space group *Imma*,[21] however, a subsequent refinement from high-resolution synchrotron X-ray powder diffraction data[16] suggested lowering of symmetry to the non-centrosymmetric *Im2a*; loss of the mirror plane perpendicular to the short axis allows elimination of some unreasonable Si–O–Si bond angles. We have chosen to adopt this lower symmetry space group in our own refinements. A typical Rietveld plot is given in Fig. 3. Final refined atomic parameters at the lowest and highest temperatures studied are given in Tables 3 and 4. The structure of CIT-5 comprises 14-membered ring channels running along the short axis [010]. Labelled plots of the framework along [010] and [001] are given in Fig. 4 and 5, respectively. Treatment of the SiO_4 tetrahedra as semi-rigid, by the application of restraints, allows flexibility in the Si–O–Si bond angles, and it is these parameters which may be anticipated to show the most variation *versus* temperature. They are plotted in Fig. 6. It can be clearly seen that the angles Si2–O1–Si4 and Si2–O10–Si4 vary the most. Fig. 4 shows that these angles are situated along the *b*-axis, and are largely responsible for driving its expansivity. Also significant is the behaviour of the Si3–O2–Si5, Si1–O3–Si1, Si1–O7–Si1 and Si3–O9–Si5 angles (Fig. 6). At first glance, these angles appear to have little correlation with the *b*-axis. However, the angle between each of the Si–Si vectors and the *b*-axis has been calculated, and the results are given in Table 5. From this, it is clear that the *b*-axis expansion is driven by the behaviour of the angles Si2–O1–Si4, Si3–O2–Si5, Si1–O3–Si1, Si1–O7–Si1, Si3–O9–Si5 and Si2–O10–Si4, whereas the angles Si4–O5–Si5, Si2–O5–Si3, Si1–O6–Si5 and Si3–O8–Si3 lie almost perpendicular to the *b*-axis, in the *ac* plane. The *a* and *c*-axis expansion is driven largely by the Si1–O6–Si5 angle.

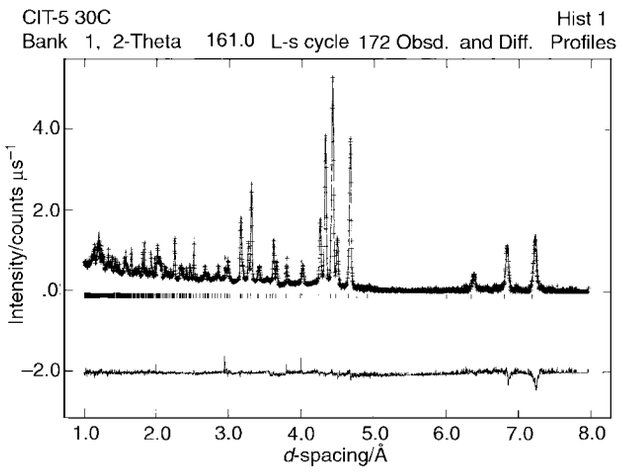

Fig. 3 Powder neutron diffraction Rietveld fit for CIT-5 at 30 °C.

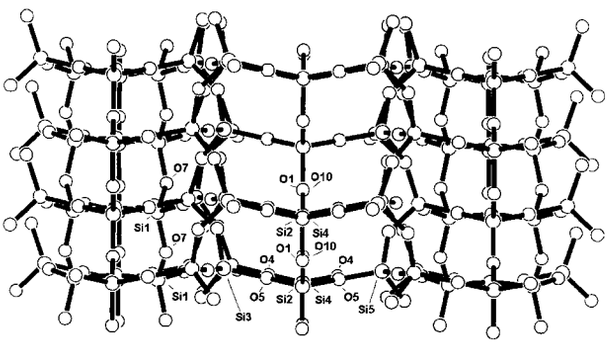

Fig. 4 Portion of the CIT-5 structure viewed along [010].

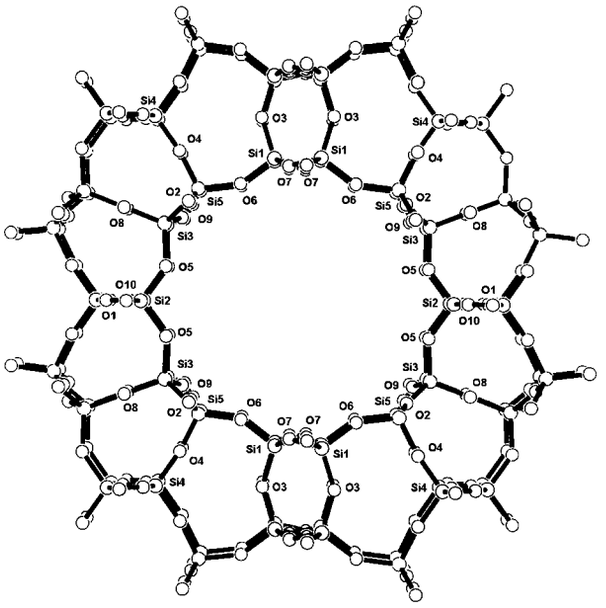

Fig. 5 14-Membered ring in CIT-5 viewed along [001].

Conclusions

The growing list of thermal expansivity data available on microporous solids clearly suggests that negative thermal expansivity is the norm rather than the exception. Of the 17 materials so far characterised, 15 show a volume contraction on heating, of which 13 show NTE along all three crystallographic axes. Only two materials, CIT-5 and $AlPO_4$-31, show

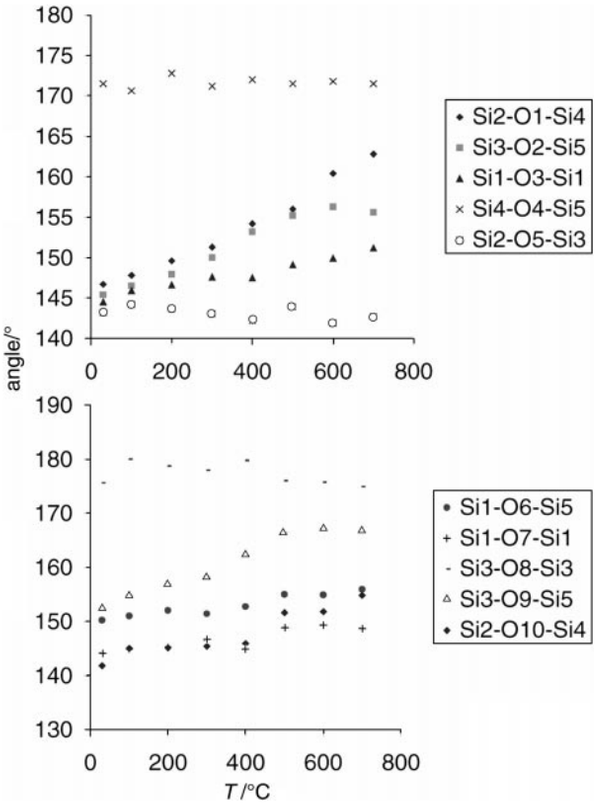

Fig. 6 Thermal behaviour of the bridging Si–O–Si bond angles in CIT-5.

Table 3 Final refined atomic parameters for CIT-5 at 30 °C; space group *Im*2*a*, $a = 13.6824(2)$, $b = 5.0214(1)$, $c = 25.5223(4)$ Å, $V = 1753.50(4)$ Å^3, $\chi^2 = 2.71$, $R_{wp} = 0.051$, $R_p = 0.11$, $R_{F^2} = 0.055$

	x	*y*	*z*	$U_{iso} \times 100$/Å^2	Multiplicity
Si1	0.6378(3)	0.506(1)	0.7162(2)	−0.09(7)	8c
Si2	0.25	0.019(1)	0.5240(2)	−0.09(7)	4b
Si3	0.4588(3)	−0.0959(9)	0.5580(1)	−0.09(7)	8c
Si4	0.25	0.522(1)	0.4564(3)	−0.09(7)	4b
Si5	0.5537(3)	0.4093(9)	0.6050(2)	−0.09(7)	8c
O1	0.25	0.3207(9)	0.5037(2)	0.07(5)	4b
O2	0.4747(3)	−0.3859(9)	0.5820(2)	0.07(5)	8c
O3	0.75	0.4754(9)	0.6981(2)	0.07(5)	4b
O4	0.6563(2)	0.4703(8)	0.5786(1)	0.07(5)	8c
O5	0.3441(2)	−0.0349(9)	0.5600(2)	0.07(5)	8c
O6	0.5690(3)	0.4451(9)	0.6666(2)	0.07(5)	8c
O7	0.6154(3)	0.7987(9)	0.7375(2)	0.07(5)	8c
O8	0.5	−0.0839(9)	0.5	0.07(5)	4a
O9	0.5172(3)	0.1125(8)	0.5933(2)	0.07(5)	8c
O10	0.25	0.3254(9)	0.0259(3)	0.07(5)	4b

Table 4 Final refined atomic parameters for CIT-5 at 700 °C; space group *Im*2*a*, $a = 13.7481(3)$, $b = 5.1068(1)$, $c = 25.6350(7)$ Å, $V = 1799.81(7)$ Å^3, $\chi^2 = 4.18$, $R_{wp} = 0.056$, $R_p = 0.059$

	x	*y*	*z*	$U_{iso} \times 100$/Å^2	Multiplicity
Si1	0.6390(4)	0.4683(9)	0.7177(3)	3.7(2)	8c
Si2	0.25	−0.0076(9)	0.5253(3)	3.7(2)	4b
Si3	0.4599(5)	−0.0568(9)	0.5574(2)	3.7(2)	8c
Si4	0.25	0.4953(9)	0.4563(4)	3.7(2)	4b
Si5	0.5515(5)	0.4494(9)	0.6061(3)	3.7(2)	8c
O1	0.25	0.2713(9)	0.4982(4)	3.1(1)	4b
O2	0.4889(7)	−0.3055(9)	0.5910(4)	3.1(1)	8c
O3	0.75	0.4668(9)	0.7023(3)	3.1(1)	4b
O4	0.6544(4)	0.4847(9)	0.5783(2)	3.1(1)	8c
O5	0.3436(4)	−0.0422(9)	0.5601(2)	3.1(1)	8c
O6	0.5742(4)	0.4366(9)	0.6664(2)	3.1(1)	8c
O7	0.6103(4)	0.7358(9)	0.7449(4)	3.1(1)	8c
O8	0.5	−0.0705(9)	0.5	3.1(1)	4a
O9	0.4974(7)	0.1948(9)	0.5875(4)	3.1(1)	8c
O10	0.25	0.2821(9)	0.0204(4)	3.1(1)	4b

Table 5 Location, thermal behaviour and directional nature of the Si–O–Si bond angles in CIT-5

Angle	Description of location	Tilt from [010] of Si–Si vector	Change in Si–O–Si *vs. T*
Si2–O1–Si4	*b*-axis	34.8°	+16.1°
Si3–O2–Si5	ring	35.2°	+10.2°
Si1–O3–Si1	bridging	34.6°	+6.7°
Si4–O4–Si5	bridging	78.8°	0°
Si2–O5–Si3	ring	78.8°	−0.5°
Si1–O6–Si5	ring	80.1°	+5.7°
Si1–O7–Si1	ring	34.6°	+4.6°
Si3–O8–Si3	bridging	88.7°	−0.7°
Si3–O9–Si5	ring	35.2°	+14.2°
Si2–O10–Si4	*b*-axis	35.8°	+13°

an overall volume expansion. Based on gross structural features, it appears that positive thermal expansivity is favoured by a high framework density (over 18 T atoms per 1000 Å^3) and a one-dimensional channel system. However, this empirical rule remains to be borne out by further studies of axial expansivities for a wider variety of framework types and compositions, including comparisons of as-made and calcined materials, and also by more detailed structural studies by single crystal diffraction methods and further computational studies. The complexity of the problem is illustrated by the observation of a positive expansivity along the channel axis in the one-dimensional 12MR system ITQ-4, but a corresponding negative expansivity in the one-dimensional 10MR system ITQ-9 (Table 2), both structures having similar framework density. The mechanism of NTE in specific microporous materials, therefore, remains unclear, although recent computational developments have suggested that certain cases can be modelled with reasonable reliability. The RUM models which have been successfully applied to β-quartz,[23] for example, have recently been extended to microporous polymorphs.[24] Gale has also recently developed analytical free energy minimisation methods[25] which he used to predict NTE in MCM-22 (MWW structure, as for ITQ-1) and SSZ-42 (IFR structure, as for ITQ-4). Further developments in these methods, alongside experimental data, will be essential for the full understanding of this unusual behaviour.

In the case of CIT-5, where positive expansivity is observed along all three crystallographic axes, the particularly large expansivity along the 14MR channel axis ($\alpha_b = 28.2 \times 10^{-6}\,^{\circ}C^{-1}$) is shown to be driven by dramatic changes in the interpolyhedral Si–O–Si angles. This effect obviously cannot, and need not, be explained merely by a dynamic rocking of tetrahedra, or a transverse vibrational mode. However, with the limited structural data available so far (specifically the powder X-ray study of $AlPO_4$-17[11] and the powder neutron study of chabazite[13]) we still cannot say whether the mechanism driving NTE in these materials has a static or dynamic origin. To discriminate between these options, higher quality, single crystal diffraction data are required. Such studies are currently ongoing.

Acknowledgements

We would like to that the EPSRC for provision of a Project Studentship (D. A. W.). Samples of the siliceous zeolites were prepared by L. A. Villaescusa and M.-J. Díaz Cabañas, in the laboratory of Dr M. A. Camblor (Valencia). We are grateful to Drs R. I. Smith and D. Engberg for help with collection of neutron diffraction data at ISIS.

References

1 J. S. O. Evans, *J. Chem. Soc., Dalton Trans.*, 1999, 3317.
2 J. S. O. Evans, T. A. Mary, T. Vogt, M. A. Subramanian and A. W. Sleight, *Chem. Mater.*, 1996, **8**, 2809.
3 J. S. O. Evans, W. I. F. David and A. W. Sleight, *Acta Crystallogr., Sect. B*, 1999, **55**, 333.
4 V. Korthuis, N. Khosrovani, A. W. Sleight, N. Roberts, R. Dupree and W. W. Warren, *Chem. Mater.*, 1995, **7**, 412.
5 D. A. Woodcock, P. Lightfoot and C. Ritter, *Chem. Commun.*, 1998, 107.
6 D. A. Woodcock and P. Lightfoot, *J. Mater. Chem.*, 1999, **9**, 2907.
7 P. Tschaufeser and S. C. Parker, *J. Phys. Chem.*, 1995, **99**, 10609.
8 J. W. Couves, R. H. Jones, S. C. Parker, P. Tschaufeser and C. R. A. Catlow, *J. Phys.: Condens. Matter*, 1993, **5**, L329.
9 S. H. Park, R. W. G. Kuntsleve, H. Graetsch and H. Gies, *Stud. Surf. Science Catal.*, 1997, **105**, 1989.
10 M. P. Attfield and A. W. Sleight, *Chem. Commun.*, 1998, 601.
11 M. P. Attfield and A. W. Sleight, *Chem. Mater.*, 1998, **10**, 2013.
12 D. A. Woodcock, P. Lightfoot, P. A. Wright, L. A. Villaescua, M.-J. Díaz Cabañas and M. A. Camblor, *J. Mater. Chem.*, 1999, **9**, 349.
13 D. A. Woodcock, P. Lightfoot, L. A. Villaescusa, M.-J. Díaz Cabañas, M. A. Camblor and D. Engberg, *Chem. Mater.*, 1999, **11**, 2508.
14 L. A. Villaescusa, P. A. Barrett and M. A. Camblor, *Angew. Chem., Int. Ed.*, 1999, **38**, 1997.
15 L. A. Villaescusa, P. A. Barrett and M. A. Camblor, *Chem. Commun.*, 1998, 2329.
16 P. A. Barrett, M.-J. Díaz Cabañas, M. A. Camblor and R. H. Jones, *J. Chem. Soc., Faraday Trans.*, 1998, **94**, 2475.
17 H. L. Zubowa, M. Richter, U. Roost, B. Parlitz and R. Fricke, *Catal. Lett.*, 1993, **19**, 67.
18 G. W. Noble, P. A. Wright, P. Lightfoot, R. E. Morris, K. J. Hudson, Å. Kvick and H. Graafsma, *Angew. Chem., Int. Ed. Engl.*, 1997, **36**, 81.
19 A. C. Larson and R. B. Von Dreele, Los Alamos National Laboratory Report No. LA-UR-86-748, 1987
20 J. M. Bennett and R. M. Kirchner, *Zeolites*, 1992, **12**, 338.
21 D. Martin and D. Engberg, *Physica B*, 1999, **134**, 268.
22 P. Wagner, M. Yoshikawa, M. Lovallo, K. Tsuji, M. Tsapatsis and M. E. Davis, *Chem. Commun.*, 1997, 2179.
23 M. B. Smirnov, *Phys. Rev. B*, 1999, **59**, 4036.
24 K. D. Hammonds, V. Heine and M. T. Dove, *J. Phys. Chem. B*, 1998, **102**, 1759.
25 J. D. Gale, *J. Phys. Chem. B*, 1998, **102**, 5423.
26 International Zeolite Association structure code, see: http://www.kristall.ethz.ch/IZA-SC/.